PERGAMON

Vision Research 38 (1998) 3857–3870

Vision Research

Optical, receptoral, and retinal constraints on foveal and peripheral vision in the human neonate

T. Rowan Candy [a,*], James A. Crowell [b], Martin S. Banks [a]

[a] *School of Optometry, University of California, Berkeley, CA 94720-2020, USA*
[b] *Division of Biology, California Institute of Technology, CA, USA*

Received 25 February 1997; received in revised form 12 December 1997

Abstract

We examined the properties of the foveal, parafoveal, and near peripheral cone lattice in human neonates. To estimate the ability of these lattices to transmit the information used in contrast sensitivity and visual acuity tasks, we constructed ideal-observer models with the optics and photoreceptors of the neonatal eye at retinal eccentricities of 0, 5, and 10°. For ideal-observer models limited by photon noise, the eye's optics, and cone properties, contrast sensitivity was higher in the parafovea and near periphery than in the fovea. However, receptor pooling probably occurs in the neonate's parafovea and near periphery as it does in mature eyes. When we add a receptor-pooling stage to the models of the parafovea and near periphery, ideal acuity is similar in the fovea, parafovea, and near periphery. Comparisons of ideal and real sensitivity indicate that optical and receptoral immaturities impose a significant constraint on neonatal contrast sensitivity and acuity, but that immaturities in later processing stages must also limit visual performance.

Keywords: Infant; Retinal eccentricity; Visual efficiency; Contrast sensitivity; Acuity

1. Introduction

The human fovea is distinctly immature at birth: The size, shape, and spacing of foveal cones differ dramatically between the adult and newborn [1,2]. Since the mature fovea is specialised for detailed vision, it is not surprising that grating acuity, vernier acuity, and contrast sensitivity at intermediate and high spatial frequencies are significantly lower in neonates than in adults [3,4].

The neonatal parafovea and near periphery appear anatomically more mature; in particular, cones and rods are reasonably adult-like [1,5,6]. Indeed, it has been hypothesized that the neonatal parafovea might be better suited to visual resolution and contrast sensitivity tasks than the neonatal fovea [7–14]. Here we examine the morphology of foveal, parafoveal, and near-peripheral human cones to estimate the spatial visual information losses that result from receptor immaturities at different retinal eccentricities.

* Corresponding author. Tel.: +1 415 5611676; e-mail: rowan@skivs.ski.org.

0042-6989/98/$19.00
PII: S0042-6989(98)00080-7

Yuodelis and Hendrickson [2] described the foveal morphology of a single 5-day-old human eye. The rod-free zone (~ 5° of visual angle) was much larger than in adults (~ 2°) and the inner retinal layers were not displaced peripherally as they are in the adult. The cone inner segments were also much wider and shorter in the neonate and the outer segments were much shorter (Table 1).

The inner segment morphology of young foveal cones has two important functional implications. First, a larger inner segment diameter implies that the spacing between cones must be greater than in adults. This reduces the highest spatial frequency that can be resolved without distortion due to spatial under-sampling. Second, inner segments with this shape cannot deliver photons efficiently to the photopigment in the outer segments. Banks and Bennett [15] quantitatively modeled the waveguide properties of these immature inner segments and found that the effective cone aperture is probably the narrower outer segment. In the adult, the aperture is in the inner segment, close to the external limiting membrane [16,17]. This combination of increased cone spacing and smaller cone aperture in

Table 1
Ideal observer parameters

Adult parameters (Data source)	Adult values Fovea	5°	10°	Infant parameters (Data source)	Infant values Fovea	5°	10°
Pupil diameter (mm) Banks and Salapatek [49]	3.3	3.3	3.3	Pupil diameter (mm) Banks and Salapatek [49]	2.2	2.2	2.2
Posterior nodal distance (mm) Larsen [38]; Stenstrom [61]	16.7	16.7	16.7	Posterior nodal distance (mm) Larsen [38]; Stenstrom [61]	11.7	11.7	11.7
Inner segment diameter (μm) Curcio [17]	2.1	6.7	7.3	Inner segment diameter (μm) Present analysis	6.5	5	4.5
				Outer segment diameter (μm) Yuodelis and Hendrickson [2]	1.2	1.2	1.2
Cone density (cones/mm^2) Curcio et al. [41]	200 000	20 400	11 300	Cone density (cones/mm^2) Present analysis	15 000	21 500	12 500
Outer segment length (μm) Banks et al. [25]	50	28	28	Outer segment length (μm) Banks and Bennett [15]; Hendrickson and Drucker [5]	3.1	4.6	10

the infant reduces the proportion of incident photons that reach the outer segments. In addition, the photons that do enter the shorter neonatal outer segment are much less likely to yield an isomerisation (assuming the same photopigment concentration). From these observations, Banks and Bennett concluded that the newborn fovea effectively absorbs 1/350 the number of photons of the adult fovea; stated another way, they argued that a stimulus that yields 350 photon absorptions in the adult would yield one absorption in the newborn. Assuredly, this deficit in photon-absorbing ability adversely affects visual sensitivity [10,15,18].

The near-peripheral retina of the newborn appears more mature than the fovea. Hendrickson and Drucker [5] examined the parafovea and near periphery of the same 5-day-old human retina described by Yuodelis and Hendrickson [2]. They found that the parafoveal cones were more mature than those in the fovea; most significantly, the inner segments were thinner and the outer segments were longer than their foveal counterparts. The extra-foveal cone lattice, therefore, might resolve finer detail and absorb a greater proportion of incident photons than the foveal lattice, and so, the newborn's parafovea could support higher visual sensitivity and resolution than the fovea.

We examine this possibility here by constructing ideal-observer models and then comparing model performance at different retinal eccentricities. Modeling of this sort has already been used to determine the physical and physiological limits of spatial contrast sensitivity in the infant and adult, but not for the infant peripheral visual field. Banks et al. [19] constructed an ideal-observer model with the optical and cone properties of the adult fovea. They modeled the mature visual system to the point of photon absorption and compared model and human contrast sensitivity for the same stimuli over a range of spatial frequencies and luminances. They found, for sinusoids composed of a constant number of cycles[1], that ideal observer and human adult performance differed by an almost constant ratio of 20:1 across a wide range of spatial frequencies (5–40 cpd) and illuminances (3.4–340 cd/m^2). They concluded that, once summation effects are minimised, information is transmitted equally efficiently beyond photon absorption from medium to high spatial frequencies and from low to moderate photopic illuminances. In other words, the shape of the high-frequency limb of the adult foveal contrast sensitivity function (CSF) can be understood from information losses due to photon noise and in the 'front-end' stages of the visual system (but see Ref. [21]).

Several investigators have entertained the following developmental hypothesis: Suppose that for transmitting the signals needed to detect gratings, the neonatal and adult visual systems are identical except for the observed differences in the eye's optics and properties of the foveal cones. If this were the case, one should be able to predict the differences between neonatal and adult contrast sensitivity and visual acuity by calculating the information lost by the neonate's visual system through having immature optics and foveal cones [10,15,18,22–24]. Banks and Bennett, and Banks and Crowell tested this particular hypothesis by comparing infant and adult contrast sensitivity to that of ideal-observer models. They reasoned that the ratio of sensitivity of ideal adult to ideal neonatal observers should be the same as the ratio of sensitivity of human adult to human neonatal observers. In fact, the ratio of empirically-observed contrast sensitivities was generally greater than the ratio of ideal sensitivities, so Banks

[1] By using a constant number of cycles, they minimised variations in grating summation across different spatial frequencies [20].

and colleagues rejected the developmental hypothesis and concluded that an additional deficit must exist; this deficit is presumably due to immaturities at later processing stages. Brown et al. reached a similar conclusion through somewhat different reasoning. Wilson [18,24] concluded that the front-end factors could by themselves account for the observed variation in contrast sensitivity, although Banks and Crowell [22] showed that his approach actually yields the same conclusion as Banks, Brown, and colleagues (see [22] for a comparison of the models).

The studies mentioned above discuss visual sensitivity in the central visual field, but in the current paper we will examine front-end constraints in the near-peripheral visual field. Banks et al. [25] constructed ideal-observer models up to photon absorption for different retinal eccentricities in the adult. They found that relative efficiency (the ratio of adult empirical contrast sensitivity divided by adult ideal sensitivity) did not vary with eccentricity at low spatial frequencies, but that it varied significantly with eccentricity at medium and high spatial frequencies. Relative efficiency declined monotonically at spatial frequencies higher than a critical value at all eccentricities. This critical spatial frequency also decreased monotonically with increasing eccentricity. Banks and colleagues proposed that the fall in efficiency is caused by the characteristic pooling of photoreceptors onto higher-order neurons (such as retinal ganglion cells) in the parafovea and periphery [26]; they calculated the pooling area required to equate relative efficiency as a function of spatial frequency at various eccentricities. By including this receptor pooling stage in their model, Banks et al. were able to explain the variation of contrast sensitivity across a wide variety of eccentricities.

In this study we have used a similar approach to examine front-end limitations to contrast sensitivity and visual acuity in the fovea, parafovea, and near periphery of the human neonate. Specifically, we have examined the hypothesis that the parafoveal and near-peripheral cone lattices ought to yield higher visual acuity and contrast sensitivity than in the fovea. We constructed neonatal and adult ideal-observer models in the fashion of Banks and Bennett [15] and Banks and Crowell [22]. The models incorporated the optical and photoreceptor properties of the fovea, parafovea, and near periphery. Receptor convergence, in the manner of Banks et al. was then included to permit a comparison of predicted empirical performance across eccentricities.

2. Methods

We constructed ideal-observer models of the adult and neonatal foveal, parafoveal, and near-peripheral retina; the models are schematised in Fig. 1. The eccentricities modeled were approximately 0, 5, and 10°. The first stage of the models is a quantitative description of the stimuli to be discriminated: a Gabor function and a uniform field[2]. The descriptions also included photon noise. These stimuli are then passed through a series of filtering and sampling stages that represent the transmittance of the ocular media, optical image formation, photon absorption among the photoreceptors, and convergence onto higher-order retinal neurons. Finally, the resulting set of neural responses is passed to an ideal decision rule that uses the likelihood ratio to discriminate the two stimuli [27].

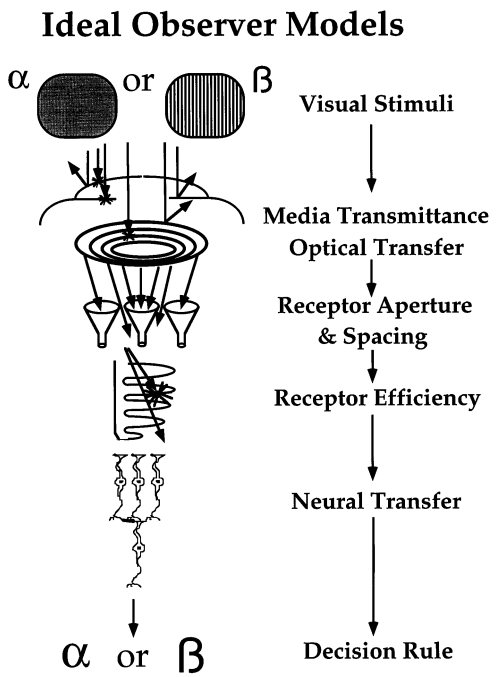

Fig. 1. Schematic of the ideal observer models. One of two stimuli—α or β—is presented to the model system. The stimuli are passed through a series of filtering and sampling stages. Finally, an ideal decision rule, based on the likelihood ratio, is used to decide whether α or β was presented.

The processing stages in the model can be summarised as follows:

$$g(x,y) = P^2 \cdot T \cdot E\{[i(x,y) * o(x,y) * r(x,y)] \cdot s(x,y)\} * n(x,y)$$

where $\cdot$ and $*$ represent multiplication and convolution, respectively, g represents the output, P represents the numerical aperture of the eye (pupil diameter divided by focal length), T represents the transmittance of the ocular media (proportion of incident photons that reach the retina), E represents the efficiency of individual receptors in converting incident photons into iso-

[2] The Gabor functions had a standard deviation of $1.6/f$ where f is spatial frequency of the patch; eight standard deviations of these functions were used.

merizations (specifically, the proportion of photons incident in the outer segments that are absorbed by the photopigment), $i(x, y)$ represents the stimulus (its luminance function), $o(x, y)$ represents the optical quality of the eye (i.e. the optical point-spread function), $r(x, y)$ represents the aperture of individual receptors, $s(x, y)$ represents the sampling function specifying the positions of receptors in the lattice, and $n(x, y)$ represents the post-receptor transfer function [22]. Ideal-observer theory is particularly appropriate for our modeling goals because its decision rule uses all of the available stimulus information, and makes no assumptions about the nature of later decision-making processes in the infant.

The parameter values incorporated into the models are given in Table 1 and the means by which they were chosen are described in the next three sections. Before discussing the specific parameters, we should describe our general strategy for setting the values. Whenever possible, parameters were given values determined by empirical observation in neonates. Otherwise, adult values were assumed. The differences in model performance are, therefore, only due to the parameters by which neonatal retinae are known to differ from adult retinae.

2.1. Optics

The retinal image formed by the eye's optics is dependent on the diameter of the pupil, the transmittance of the media, the posterior nodal distance, and the optical quality of the eye.

In particular, the quantity of light incident on a retinal patch (for example, in photons/deg^2) is proportional to the media transmittance, inversely proportional to the square of the posterior nodal distance, and proportional to the pupil area. Media transmittance is determined primarily by two structures that change in density with age: the crystalline lens and macular pigment. Both structures absorb short wavelengths chiefly, and are more transparent in the neonate than in the adult [28–30]. We assumed preretinal optical densities at 400 nm of 0.7 and 1.1 for neonates and adults, respectively [31]. The macular pigment is laid down over the first three years [28], so for neonates, we assumed an optical density of 0.00 at all eccentricities, and for adults, we assumed pigment densities at 460 nm of 0.50 in the fovea, 0.11 at 5°, and 0.03 at 10° eccentricity [28,32]. The smaller pupil area and shorter posterior nodal distance of the neonatal eye have opposing effects on retinal illumination and, as a consequence, the retinal illumination for a given light source is roughly constant for the ages modeled except for the small differences in media transmittance [33].

The optical transfer function (OTF) is a quantification of the quality of the eye's optics. Specifically, the OTF represents the degree to which different spatial frequencies in the object are passed by the optics to the retinal image. In the adult eye, the OTF is roughly constant from the fovea to 10° retinal eccentricity [34]. The OTF of the neonatal eye has not been measured, but fine fundus details are visible during ophthalmoscopic examination [35], so the optical quality of the neonatal eye must be reasonably high[3]. For these reasons, we assumed that the OTF of the neonatal eye is adult-like at the retinal eccentricities being modeled. Specifically, we used the adult OTF of Campbell and Gubisch [37] for a 3-mm pupil and white light in all of the models.

In addition to the image quality constraints described above, the size of the retinal image (in mm) is dependent on the posterior nodal distance of the eye. The posterior nodal distance of the adult eye is 16.7 mm on average [38]. The posterior nodal distance of the neonatal eye has not been measured, although the axial length is approximately 16.6 mm; roughly 2/3 of the length of the average adult eye [38]. Assuming that the posterior nodal distance is a constant fraction of the axial length, we estimate a posterior nodal distance of 11.7 mm for the neonate. Thus, for a small object at a fixed distance, the retinal image size (in mm) in the neonatal eye is about 2/3 of that in the adult eye.

2.2. Photoreceptors

A number of photoreceptor properties determine the rate of absorption of incident photons. These include the diameter of the cone aperture, the spacing between cones, and the optical density of the photopigment. At birth, the aperture and spacing appear more efficient at non-foveal sites than they are in the fovea. Hendrickson and Drucker [5] described neonatal cones and rods at 1–1.5 and at 4 mm retinal eccentricity in the 5-day-old eye described by Yuodelis and Hendrickson [2]. Their descriptions did not quantify some of the properties required for our modeling, so we made measurements in some new photographs of the same 5-day-old eye (see Fig. 2 and Appendix A).

The size of the cone aperture has two effects on processing of the retinal image. First, large apertures cause an attenuation of high-spatial-frequency information [22,39]. Second, large apertures allow individual cones to collect more light.

The spacing between cones determines the resolu-

[3] In comparison, the OTF of the kitten eye is poor and fundus details cannot be seen [36].

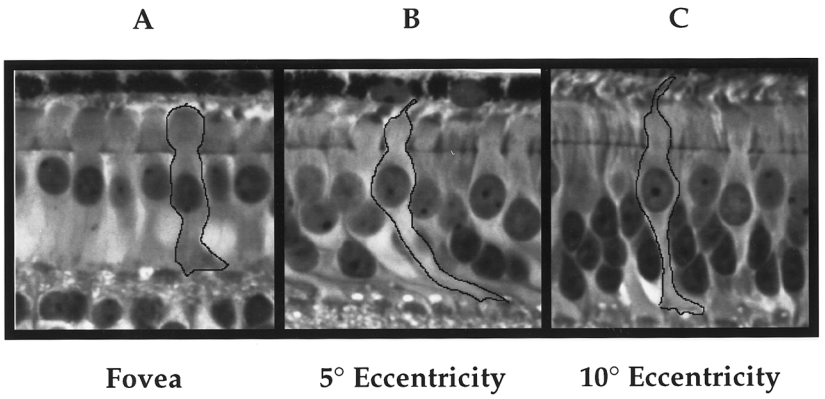

Fig. 2. Vertical sections of the 5-day-old human retina described by Yuodelis and Hendrickson [2] and Hendrickson and Drucker [5]. These are parts of new photographs taken at three retinal positions. (A) The center of the fovea; (B) 900 μm from the center of the fovea nasally (~ 5° retinal eccentricity); (C) 1800 μm from the foveal center nasally (~ 10° eccentricity). One cone has been outlined in each photograph.

tion with which the retinal image can be sampled. In the case of a regular hexagonal lattice, the highest spatial frequency that can be resolved, without spatial aliasing, is the Nyquist frequency:

$$N = \frac{1}{2 \tan^{-1}\left(\frac{\sqrt{3}}{2}\frac{S}{P}\right)}$$

where S is the spacing between receptors and P is the posterior nodal distance of the eye [40]. The Nyquist frequency is significantly lower in the neonatal than in the adult fovea [15,24], however, in the parafovea and near periphery, the Nyquist frequencies are more similar (Table 2).

Both cone aperture and spacing determine the retinal coverage [15,17], which is the proportion of retinal area covered by cone apertures. The equation for retinal coverage is: NR/A, where N is number of cones in the area of tissue being considered, R is the cone aperture area, and A is the area of tissue being considered. Retinal coverage estimates at different eccentricities are given in Table 2.

The adult values for cone spacing and aperture diameter were derived from Curcio et al. [41] and Curcio [17], respectively. We assumed a regular hexagonal lattice in order to convert the cone densities reported by Curcio et al. [41] into inter-cone spacings. The aperture diameters were taken directly from Curcio [17] (see also, [16]).

The location of the cone aperture in infant cones is not known. Banks and Bennett [15] modeled waveguide effects in neonatal foveal cones using geometric optics approximations. As stated above, they concluded that the inner segment dimensions are not appropriate for funneling photons and that, consequently, the outer segment appears to contain the effective aperture. Brown et al. [10] arrived at the same conclusion by somewhat different reasoning. We, therefore, assumed that the outer segment is the effective aperture in the foveal model. Parafoveal and near-peripheral cones are more mature anatomically than foveal cones and, so, their inner segments may contain the effective aperture. As the evidence is not clear on this issue, we decided to model both of the two most extreme possibilities in our non-foveal models. Specifically, we based separate calculations on assumptions that: (1) the inner segment at the external limiting membrane is the effective aperture; and that (2) the outer segment is the effective aperture. The inner segment diameters were measured directly from the photographs of the 5-day-old eye. The widths of the 'full cut' receptors (Fig. A1, part C) were measured at a level where, on average, the inner segments were widest. These measurements were then averaged across approximately 1° of tissue. Hendrickson and Drucker [5] did not report significant changes in neonatal outer segment diameters with eccentricity and the diameter did not appear to vary in the new photographs. Therefore, we used Yuodelis and Hendrickson's [2] value of 1.2 μm as the infant outer segment diameter at all eccentricities.

No estimates of receptor spacing at extrafoveal sites have been reported in the infant literature, so we made new spacing calculations. In the work of Hendrickson et al., the 5-day-old eye had been sectioned parallel to the long axis of the photoreceptors. Yuodelis and Hendrickson [2] estimated cone packing density from these vertical sections and, as described in Appendix A, this method may over-estimate the density. We used a new method (also described in Appendix A) to estimate cone packing density from which the average cone spacing can be calculated.

The proportion of incident photons that are effectively absorbed also depends on the optical density of the photopigment. Pigment optical density in turn depends on the concentration and extinction coefficient of the photopigment and on the length of the outer segment. These relations are described by the Beer–Lam-

Table 2
Calculated receptor properties

Property	Adult			Infant		
	Fovea	5°	10°	Fovea	5°	10°
Cone spacing (min)	0.49	1.5	2.1	2.6	2.2	2.8
Nyquist limit (cpd)	70	22	16.5	13.5	16	12
Retinal coverage						
Inner segment	0.69	0.71	0.47	—	0.42	0.21
Outer segment				0.016	0.024	0.014
Proportion isomerizations						
Inner segment	0.45	0.32	0.21	—	0.038	0.039
Outer segment				0.0011	0.0022	0.0026

bert law [32]. The concentration and extinction coefficient of neonatal photopigment are unknown, so we assumed that they are adult-like. The specific values chosen were from Banks and Bennett [15]; they did not vary with retinal eccentricity or age. We could not measure neonatal outer segment lengths reliably in the new photographs, so we used Yuodelis and Hendrickson's foveal and foveal slope estimates for the foveal and 5° models, respectively. The 10° neonatal estimate was derived from Hendrickson and Drucker's measurements at an eccentricity of 1.5 mm ($\sim 8°$). The adult outer segment lengths were taken from Banks and Bennett [15].

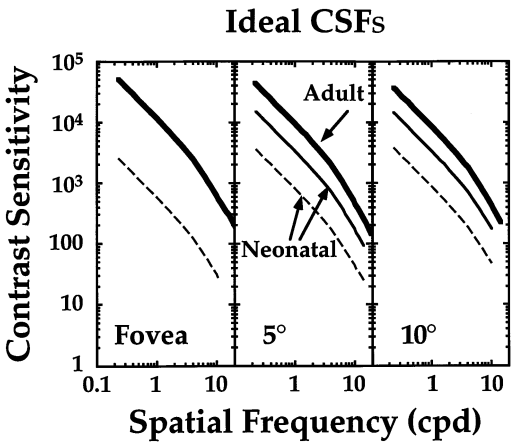

Fig. 3. Adult and neonatal ideal CSFs. The panels display functions at the fovea and at 5 and 10° retinal eccentricity. Each panel contains adult and neonatal functions for models limited only by photon noise, the optics, and cone properties. The thick lines represent the adult functions and the thin lines the neonatal functions. There are two neonatal functions at the non-foveal eccentricities: The continuous lines represent functions for models with inner segment apertures and the dashed lines represent functions for models with outer segment apertures. The functions are truncated at the Nyquist frequency for each eccentricity considered.

2.3. Receptor convergence

In the primate fovea, there are many more post-receptoral retinal neurons than photoreceptors; for example, there are three or four retinal ganglion cells for every foveal cone [26,41]. With increasing retinal eccentricity, however, the ratio of post-receptoral neurons divided by cones decreases monotonically. A significant consequence of the changing ratio of neurons/cones is a change in the number of cones feeding the center mechanism of retinal ganglion cells. In the periphery, dozens of cones may provide input to the center mechanism of one ganglion cell. The functional consequence of such receptor convergence is a loss in the ability to transmit high-spatial-frequency information [25,42–44].

In their analyses of optical/receptor limitations to spatial vision, Banks and Bennett [15] and Banks and Crowell [22] assumed that the decision-making device has access to signals from individual cones. This assumption is reasonable for the fovea, but not for parafovea or near periphery. Thus, models of spatial vision at extrafoveal loci commonly assume that the inputs from several cones are pooled at higher-order retinal neurons [25,43].

There are, of course, no measurements of receptor pooling in the human infant, but there are two forms of evidence suggesting that such pooling exists early in life. First, connections between receptors and higher-order retinal neurons are established before birth [2,6]. During infancy, the receptors migrate toward the fovea and other retinal neurons migrate away from the fovea [2], however, it appears that the connections between receptors and higher-order retinal neurons are maintained [6,45]. Consider in the neonate a patch of receptors connected to higher-order neurons. As the patch migrates toward the fovea, the spacing between individual receptors decreases such that the visual angle that patch subtends decreases over time. However, as the

patch migrates toward the fovea, its retinal eccentricity also decreases over time. If we assume that receptor pooling is a linear or nearly linear function of retinal eccentricity, these two effects of migration cancel each other such that pooling diameter (in degrees) remains constant. The second form of evidence comes from anatomical and physiological studies of retinal development in other mammalian species. These studies have found that the diameters of ganglion cell receptive fields are, if anything, larger in kittens than in cats [46,47]. Evidence in infant primates comes from a physiological study of the spatial receptive field properties of LGN cells [48]. The highest spatial frequency to which LGN cells respond depends both on age and retinal eccentricity, yet the resolution of the extrafoveal cells is similar across age. This is consistent with the idea that resolution of extrafoveal cells is limited by a process that does not change with age. Because the primary limit to resolution in the periphery of the adult is receptor pooling, these observations suggest that pooling (expressed in units of visual angle) at a given eccentricity does not change with age. For this reason, we have chosen to include a receptor-pooling stage in our ideal-observer models of the neonatal parafovea and near periphery (and the adult extrafoveal models as well). We constructed models with no pooling for comparison.

Receptor pooling values were estimated using the method and adult contrast sensitivity measurements described in Banks et al. [25]. The pooling stage was represented by a Gaussian of unit height. Pooling was varied by varying the standard deviation of the Gaussian in order to equate the slopes of the high-frequency limbs of the ideal and human adult CSFs. The Gaussian providing the best fit was then incorporated into the ideal-observer model at the appropriate retinal eccentricity. The standard deviations of the filters were 2.62 and 3.52 min at 5 and 10°, respectively.

2.4. Model performance

We calculated CSFs for each of the models and compared these functions to the appropriate human data from adults and neonates. The ideal observer CSFs were derived using the same 2-alternative, forced-choice task as presented to the adult observers in Banks et al. [25]. In all instances, the ideal observer was required to discriminate the Gabor patch of constant number of cycles from a uniform field. Contrast thresholds were defined as the contrast required for $d' = 0.96$. The results were compared with the human adult data from Banks et al. [25]. The human neonatal data were from Banks and Salapatek [49], which was an FPL study, and from Norcia et al. [50], which was a VEP study.

The ideal CSFs were calculated for a mean luminance of 50 cd/m^2, and Banks and Salapatek [49] collected their data at 55 cd/m^2; these correspond to retinal illuminances of $\sim$400 Td. Banks et al. [25] and Norcia et al. [50], however, collected their data at $\sim$1300 and 1700 Td, respectively. These differences in the effective illuminances among the studies must be taken into account before one can compare their results. This requires an assumption about how variations in retinal illuminance affect contrast sensitivity. The range of plausible assumptions varies from square-root law (contrast sensitivity is proportional to the square-root of illuminance) to Weber's law (sensitivity is independent of illuminance). Human adults exhibit both forms of behavior depending on the stimulus parameters; the general rule is that Weber's law predominates at high illuminances and low spatial frequencies. In particular, Weber's law is observed in the fovea for illuminances greater than 300–400 Td and spatial frequencies less than 5 cpd [19,51], and Weber's law is observed at somewhat lower illuminances in the near periphery [52,53]. We, therefore, assumed that adults follow Weber's law at the eccentricities and illuminances considered here, and the adult data were, for this reason, not shifted to compensate for differences in retinal illuminance among the empirical studies. There is no data on the relationship between contrast sensitivity and illuminance in neonates at the illuminance used by Norcia et al. [50], although Shannon et al. [33] found that 2-month olds nearly followed square-root law at 1000 Td, so we assumed that square-root law should be used to shift neonatal data. Once these data were made equivalent in retinal illuminance, we could consider the differences between them in terms of sensitivity differences within the visual system (in particular, photon catch).

3. Results and discussion

We first examined the contrast sensitivity of adult ideal and neonatal ideal observers limited only by photon noise, the optics, and cone properties; there was no receptor pooling in these models. The functions displayed in the three panels of Fig. 3 show ideal CSFs for retinal eccentricities of 0, 5, and 10°. The adult functions are represented by the thick lines and the neonatal functions by the thin continuous and dashed lines. At 5 and 10°, the neonatal functions were calculated for two different modeling assumptions: one assuming inner segment apertures (continuous lines) and the other assuming outer segment apertures (dashed lines).

We have plotted sensitivities only below the Nyquist limit at the relevant eccentricities (Table 2) even though the ideal observer models can perform the discrimination task above the Nyquist limit using spatial aliases.

Fig. 3 shows that there is little change in ideal adult sensitivity between 5 and 10° eccentricity and that the foveal model is somewhat more sensitive than the non-foveal models at all spatial frequencies.

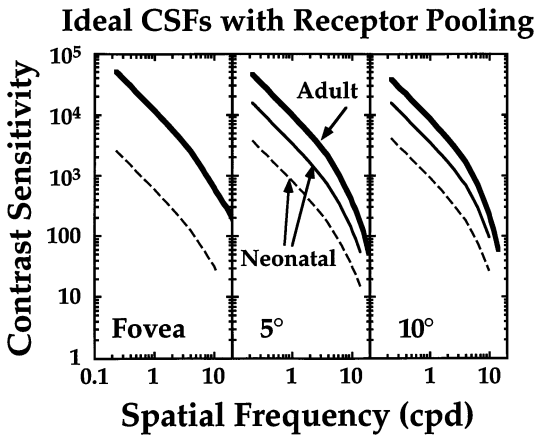

Fig. 4. Adult and neonatal ideal CSFs with receptor pooling. The panels display functions at the fovea and at 5 and 10° retinal eccentricity. The thick lines represent the adult functions and the thin lines the neonatal functions. There are two neonatal functions at the non-foveal eccentricities: the continuous lines represent functions for models with inner segment apertures and the dashed lines represent functions for models with outer segment apertures. No receptor pooling is assumed for the foveal functions, so they are identical to the foveal functions in Fig. 3. The functions are again truncated at the Nyquist frequency for each eccentricity considered.

Ideal infant sensitivity varies more with eccentricity. The assumed cone aperture has two effects on ideal contrast sensitivity. First, larger apertures enable a greater photon catch, thereby reducing the effective photon noise. This effect is most noticeable in Fig. 3 as an increase in contrast sensitivity for the inner segment functions relative to the outer segment functions. Second, larger apertures yield more spatial averaging which in turn yields a reduction in the ability to transmit high-spatial-frequency information. This effect is most noticeable in Fig. 3 as a slightly steeper high-frequency slope in the inner segment functions. This effect would be more apparent if sensitivities for frequencies above the Nyquist limit were plotted.

The models can detect the presence of gratings with spatial frequencies well above the Nyquist limit of the receptor lattice (Table 2), however, model performance is not plotted at those frequencies due to its dependence on the assumed regularity of the lattice and the spatial phase and orientation of the stimulus relative to the lattice. It might seem surprising initially that detection can occur well above the Nyquist limit, but it only demonstrates that the ideal observer is able to use information from spatial aliases when asked to discriminate between a Gabor function and a uniform field.

In regard to variation in performance with retinal eccentricity, the infant models show little difference between 5 and 10° eccentricity. However, unlike the adult models, the extra-foveal infant models are more sensitive than their foveal equivalent. This finding is similar to an outcome of Brown's [9] modeling of the front end of the neonatal visual system. Brown estimated that the cone lattice of the parafovea of the young eye absorbs about 23 times more photons than the foveal lattice and argued, therefore, that the parafovea ought to support higher contrast sensitivity and visual acuity than the fovea. Brown only analyzed the properties of the cone lattices and, therefore, did not include eccentricity-dependent variations in receptor pooling in her calculations.

For reasons stated earlier, the assumption that no receptor pooling exists in the peripheral retina of human neonates is implausible. Rather it is more likely that the convergence (expressed in units of visual angle) in neonates of cones onto higher-order retinal neurons is similar to the convergence in the mature visual system [25,26]. Thus, we constructed ideal-observer models with adult-like receptor pooling at each retinal eccentricity.

The functions displayed in the three panels of Fig. 4 show the CSFs of these models for retinal eccentricities of 0, 5, and 10°. The adult functions are represented by the thick lines and the neonatal functions by the thin lines. The foveal functions are the same as those in Fig. 3 because we assumed that no pooling occurs at that eccentricity. The non-foveal, neonatal functions were again calculated for two modeling assumptions: inner segment apertures and outer segment apertures.

The consequence of adding receptor pooling at eccentricities of 5 and 10° can be seen by comparing Figs. 3 and 4. The primary effect of adding a pooling stage is a reduction in sensitivity at high spatial frequencies because increasing convergence is equivalent to blurring the retinal image.

One of the main motivations for this work was to determine whether fine spatial information is likely to be signaled more reliably by the neonate's retina when the information is presented extrafoveally rather than foveally. To the extent that our modeling assumptions are reasonable, we can answer this question by comparing the sensitivities of the ideal observer models at the three retinal eccentricities. Ideal neonatal CSFs at 0, 5, and 10° are plotted in Fig. 5. The foveal function is the same in each panel since we always made the same assumptions (outer segment aperture with no receptor pooling) for the foveal models. The non-foveal functions with the highest and lowest sensitivity are plotted for each eccentricity in panels A and B, respectively. The non-foveal functions in panel A assume inner segment apertures and no receptor pooling at 5 and 10°. The functions for 5 and 10° eccentricity in panel B assume an outer segment aperture and receptor pooling. As stated earlier, the most plausible assumptions are no receptor pooling with outer segment apertures at the fovea, and adult-like pooling at 5 and 10°. There is no reasonable way to decide whether the inner or outer segment is the more likely aperture in the periphery, so

inner segment functions with receptor pooling are shown in panel C. In summary, although panels A and B show the most and least sensitive models, the most plausible models are shown in panels B and C.

The significance of the diameter of the cone aperture is evident when panels B and C are compared. When it is assumed that the outer segment is the effective cone aperture in the parafovea and near periphery (panel B), as it is in the fovea, ideal neonatal sensitivity is similar at 0, 5, and 10° at all of the plotted spatial frequencies. When it is assumed, on the other hand, that the inner segment is the effective aperture in the parafovea and near periphery (and the outer segment in the fovea, panel C), contrast sensitivity is actually lower in the fovea; the sensitivity difference decreases noticeably with increasing spatial frequency. Thus, our analysis of the optical/receptoral limits on neonatal spatial vision leads to two implications. First, assuming outer segment apertures, the fovea and supporting retinal circuits are as well-suited as the parafovea and near periphery for signaling fine spatial information. In this regard, by including a receptor-pooling stage, we come

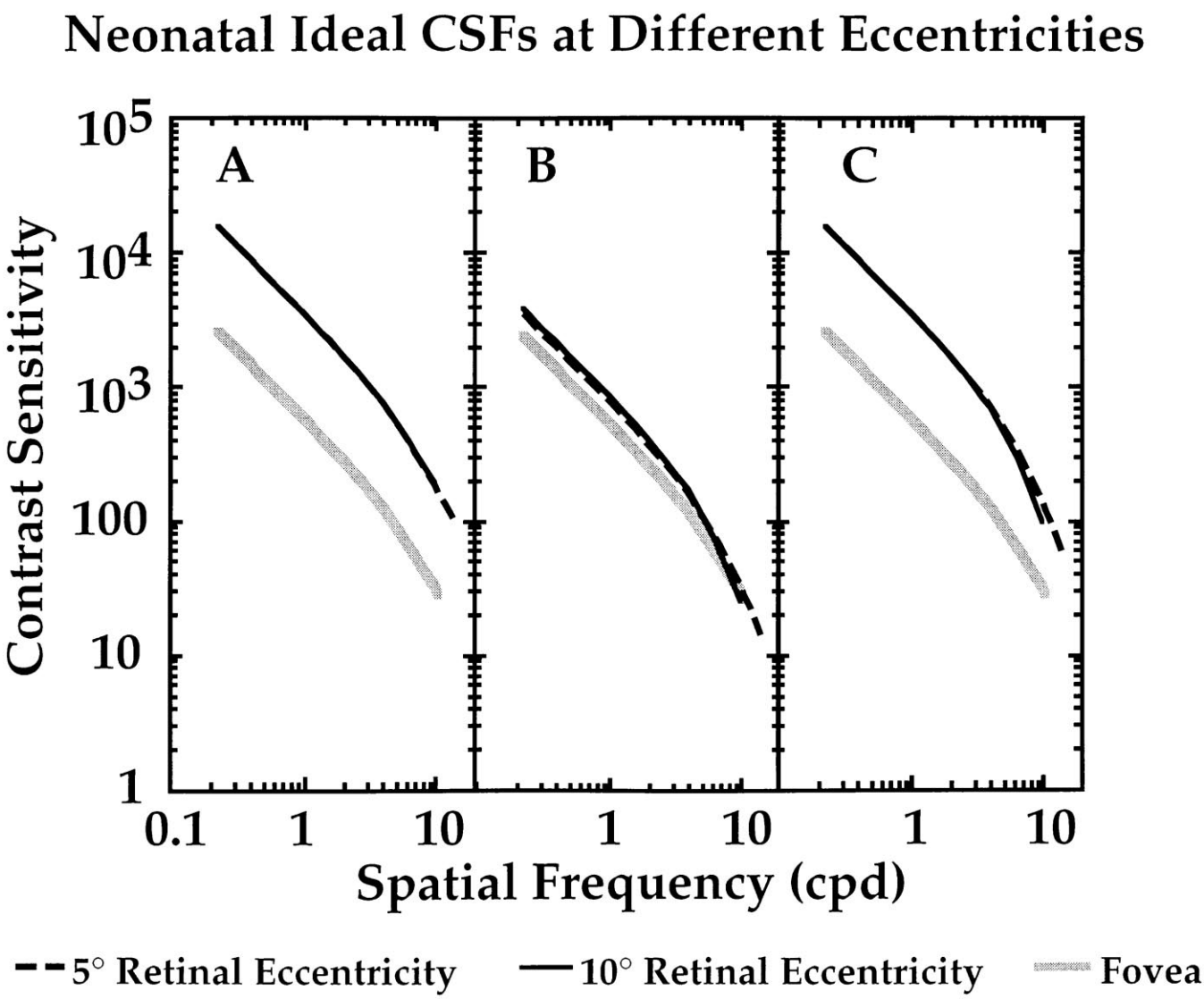

Fig. 5. Neonatal ideal CSFs for different modeling assumptions. The thick gray lines represent the foveal function (no pooling and outer segment aperture) in all panels. The dashed black lines represent functions from 5° retinal eccentricity, and the thin black continuous lines represent functions from 10° retinal eccentricity. Panels A and B display the most and least sensitive ideal CSFs for each retinal eccentricity, respectively. The most sensitive model at the non-foveal eccentricities was the inner segment receptor aperture and no receptor pooling model, and the least sensitive model incorporated an outer segment aperture with adult-like pooling for the relevant eccentricity. Although the most and least sensitive functions are shown in panels A and B, the most plausible set of assumptions are no receptor pooling and an outer segment aperture at the fovea, and adult-like pooling at 5 and 10°. There is no reasonable way to decide whether the inner or outer segment is the more likely aperture extrafoveally, so inner segment aperture functions with receptor pooling are shown in panel C; although panels A and B show the most and least sensitive models, the most plausible models are shown in panels B and C.

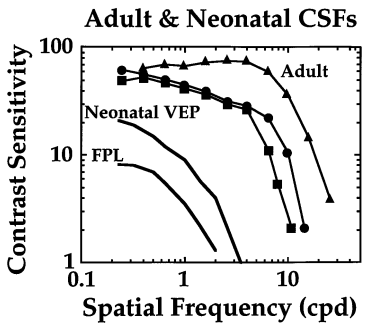

Fig. 6. Empirically-observed adult and neonatal CSFs. Adult data are represented by the curves with symbols. They are from observer ABS in Banks et al. [25] at eccentricities of 0° (triangles), 5° (circles), and 10° (squares). The neonatal data are represented by the solid curves in the lower left. The VEP data are from Norcia et al. [50] and the FPL data are from Banks and Salapatek [49]. The VEP data have been shifted by the square-root of the ratio of luminances in the FPL and VEP studies in order to make the curves comparable in photon catch.

to a different conclusion than Brown [9]. Second, assuming inner segment apertures, the parafovea and near periphery, and supporting retinal circuits, are better suited to signaling coarse spatial information (e.g., spatial frequencies lower than 5 cpd) and might be better suited to signaling fine detail as well. Clearly, a determination of the site of the effective cone aperture is crucial to pinning down the front end constraints on neonatal spatial vision.

We next examine the developmental hypothesis that the only differences between the neonatal and adult visual systems (by which we mean those parts of the system that are relevant to performance in contrast sensitivity and visual acuity experiments) are the immaturities evident in the optics and cones. This is the same hypothesis described by Banks and Bennett [15] and Wilson [18], however, we also examine the possibility that the neonate uses the parafovea and/or near periphery in contrast sensitivity and acuity experiments [8,14]. If the acuity and contrast sensitivity reductions observed in neonates were due only to differences in the front end, then we should be able to predict the empirical observations by calculating the information losses from front-end immaturities (as depicted in Fig. 5) and then applying those losses to the contrast sensitivities and acuities observed in adults.

Fig. 6 displays empirically-observed CSFs of adults and neonates. The three adult functions are for retinal eccentricities of 0, 5, and 10°; the two neonatal functions are based on forced-choice preferential looking (FPL) and visual-evoked potential (VEP) measurements at unknown retinal eccentricities. The adult data are from one observer in Banks et al. [25]. The neonatal FPL function is the 1-month data of Banks and Salapatek [49] and the VEP function is from the 1-month data of Norcia et al. [50]; the VEP function has been shifted downward in order to compensate for the difference in luminance in the FPL and VEP measurements, as described earlier. The disparity between the adult and neonatal functions illustrates the contrast sensitivity deficit commonly observed in young infants. In particular, adult contrast sensitivity is significantly higher than neonatal sensitivity even when the adult uses a retinal locus as far as 10° from the fovea.

We can test the developmental hypothesis that the neonatal sensitivity deficit is caused by immaturities in the front end alone by shifting the empirically-observed adult functions by the ratio of ideal neonate divided by ideal adult contrast sensitivity.

Fig. 7 displays the results of such shifts. The empirically-observed infant CSFs from Fig. 6 are displayed again as solid lines. The filled and open symbols represent the predictions; in particular, they are the functions that result from shifting adult CSFs at different retinal eccentricities by the ratios of ideal sensitivities for the infant curves shown in Panels A and B of Fig. 5. (Recall that ideal sensitivities differ in large part because the photon catch, and hence the photon noise, differs from one model to another; a dependence on photon catch yields square-root law which in turn is the primary determinant of the ratios of sensitivities in Fig.

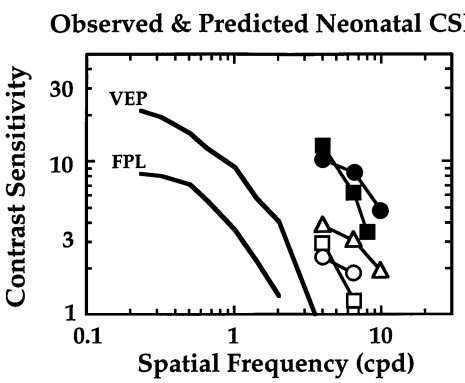

Fig. 7. Observed and predicted neonatal CSFs. The solid curves on the left represent the CSFs from the FPL study of Banks and Salapatek [49] and the VEP study of Norcia et al. [50] (Fig. 6). The curves on the right are the result of shifting empirically-observed adult CSFs (Fig. 6) by the ratio of ideal neonatal sensitivity divided by ideal adult sensitivity. The various shifted functions were obtained with different retinal eccentricities and different modeling assumptions as described in the text. Triangles represent a shift based on an adult foveal CSF and the model of the neonatal fovea. Circles represent shifts based on an adult CSF at 5° and models of the neonatal parafovea: The filled circles are based on models with inner segment apertures and no receptor pooling, and the open circles on models with outer segment apertures and eccentricity-appropriate pooling. Squares represent shifts based on an adult CSF at 10° and models of the neonatal near periphery: Filled squares are based on models with inner segment apertures and no receptor pooling, and the open squares on models with outer segment apertures and eccentricity-appropriate pooling.

5.) The unfilled symbols represent the shifts that occur when we assume outer segment apertures and adult-like pooling at all eccentricities; these particular modeling assumptions yield the lowest sensitivities (Panel B, Fig. 5). The filled symbols represent the shifts when we assume the inner segments are the apertures at 5 and 10° and that no pooling occurs; these modeling assumptions yield the highest sensitivities (Panel A, Fig. 5). We used the modeling assumptions leading to the least and most sensitive outcomes in order to show the extremes. For the set of modeling assumptions shown in Panel C, Fig. 5, the shifted functions fall in between the ones shown here. Notice that we only shifted the functions for spatial frequencies equal to or greater than 4 cpd; we did so as there is clear evidence [51] that the square-root assumption that underlies the shifting is violated for lower spatial frequencies at these luminances.

All of the shifted functions lie above the empirically-observed neonatal CSFs. This means that one cannot explain the high-frequency contrast sensitivity deficits observed in human neonates from front-end immaturities alone: Neonates' high-frequency sensitivity is even poorer than predicted whether we assume they are using the fovea, parafovea, or near periphery to perform the task. It should be noted that we made predictions of the worst performance possible in that this data shift assumes square-root law; if we used empirically-determined contrast versus illuminance functions to shift the adult data [33], the shifted functions would all lie farther above the neonatal data. We must conclude, therefore, as Banks and Bennett [15] and Banks and Crowell [22] did, that there are further immaturities at later stages of the neonatal visual system.

Over the past two decades, many investigators have argued that neonatal vision is similar to adult peripheral vision and, therefore, that assessments of neonatal vision are based primarily on stimulation of peripheral retina [7–10,12–14]. There are now two reasons to argue against this hypothesis.

The first is a set of experiments that have compared infants' visual acuity measured with foveal or near-foveal stimulation to infants' acuity observed with peripheral stimulation [54–59]. None of these studies individually provides persuasive evidence that foveal acuity is better than near-peripheral acuity in neonates because the ones that measured fixation objectively did not use conventional stimuli for measuring visual acuity and the ones that used conventional stimuli did not measure fixation. Nonetheless, these studies as a whole provide reasonably persuasive evidence that a neonate's acuity is best with central fixation.

The second reason for arguing against peripheral dominance comes from our analysis of the front-end limitations to visual resolution. The parafoveal and near-peripheral cone lattices might well absorb more photons than the foveal lattice (see our Fig. 3; [9]), however, this extra-foveal advantage is probably lost or, at least greatly reduced, once the signals are attenuated by the convergence of extra-foveal cones onto higher-order retinal neurons.

It is interesting and important to note that many of the parameters relevant to our modeling differ from one adult retina to another [41]. Naturally, the same could be true, perhaps even to a larger degree, for neonatal retinas. Given the scientific interest in understanding the limits imposed by retinal structures on the development of visual function, we hope that tissue from more than one neonate [2] will become available. Only then can we resolve the issue of how representative this particular retina is.

Acknowledgements

We thank Anita Hendrickson at the University of Washington for assisting us in photographing the 5-day-old human retinal tissue. T R Candy was supported by a William C Ezell Fellowship from the American Optometric Foundation, and the research was supported by National Institutes of Health Research Grant HD-19927.

Appendix A

The tissue examined by Hendrickson and Drucker [5] was sectioned vertically (perpendicular to the surface of the retina and therefore parallel to the long axis of the receptors), so it is difficult to determine the density and arrangement of the cone lattice from those sections. Thus, there are no published measurements that allow an estimate of cone packing density in the parafovea and near periphery of the human neonate.

Yuodelis and Hendrickson [2] estimated the packing density of foveal cones in their human infant samples by counting the number of cones visible in vertical tissue sections across the central 250 μm of the rod-free zone (see their Table 4). They assumed that the infant foveal cones are arranged in a perfectly-regular hexagonal lattice and that their vertical sections had sliced through a row of cones. As illustrated in parts A and B of Fig. A1, their technique could yield an over-estimation of the actual packing density for two reasons. First, as shown in part A, a vertical slice may not be perfectly aligned with a row of cones. In the example shown, ten cones are counted in the non-aligned slice and seven along the aligned slice; a difference of 30%. Second, as shown in part B, the over-estimation of density could be compounded by irregularity in the cone lattice. Notice that the same number of cones are counted in the non-aligned slices in parts A and B,

although the density in part B is 17% lower than the density in A. This problem of over-estimation is lessened by the observation that foetal receptor lattices are regular and hexagonal in arrangement [60].

We developed a technique for measuring cone packing density that is less affected by the assumptions of aligned slices and regular cone arrangement. With the assistance of Anita Hendrickson, we re-photographed the tissue from the 5-day-old eye examined by Yuodelis and Hendrickson [2] and Hendrickson and Drucker [5]. The tissue had been sectioned vertically at regular intervals. Three adjacent sections contained the center of the fovea and extended far into the periphery. These sections were 2 μm thick and separated by 4 μm. We photographed these three sections at the center of the fovea, at 900 μm (~ 5°) and at 1800 μm (~ 10°) nasally along the horizontal retinal meridian (Fig. 2).

The inner segment diameters were estimated by measuring the widths of the 'full cut' receptors (Fig. A1, part C) at the height at which the inner segments were the widest. These measurements were averaged across approximately 1° of tissue. In the fovea, the average diameter in all three sections was 5.5 μm (S.D. = 0.6 μm). Assuming 15% tissue shrinkage during histological fixation, the actual diameters would be ~ 6.5 μm which is consistent with the measurements reported by Yuodelis and Hendrickson [2]. At 5° eccentricity, the average inner segment diameter was 4.5 μm (S.D. = 0.5), and at 10°, the average was 4.0 μm (S.D. = 0.4). Correcting for shrinkage, the actual diameters at 5 and 10° would be ~ 5.0 and ~ 4.5 μm, respectively.

If the distance between slices is 4μm and the average inner segment diameters are 4–4.5 μm in non-foveal retina (not corrected for shrinkage), it is unlikely that a cone visible in one section would appear in another section, or that a cone would be not visible in two adjacent sections. Given this, we can estimate cone packing density by counting the total number of cones visible in the three sections and then dividing by the area of tissue from which visible cones could be drawn. The cone density (and spacing) estimates presented in Table 1 were obtained in this way.

The estimation of cone packing density is more problematic in the fovea because the inner segments are wider (5.5 μm) than the inter-section separation (4 μm). Specifically, there is now a reasonable likelihood that the same inner segment would appear in two adjacent sections. We can assess the likelihood of this occurrence, however, from the appearance of the inner segment in the section. A segment with an apparent width close to 5.5 μm must have been sliced near its center and is, therefore, unlikely to appear in another section; we call this occurrence a 'full cut' (Fig. A1, part C). A segment with a much smaller apparent width (and frequently, other material visible through it) must have been sliced near its edge and is, thus, more likely to appear in another section; we call this a 'graze cut'. In order to count each cone once, and only once, we had to determine the relative alignment of the three sections and then identify corresponding graze cuts in the neighboring sections. We determined the relative alignment

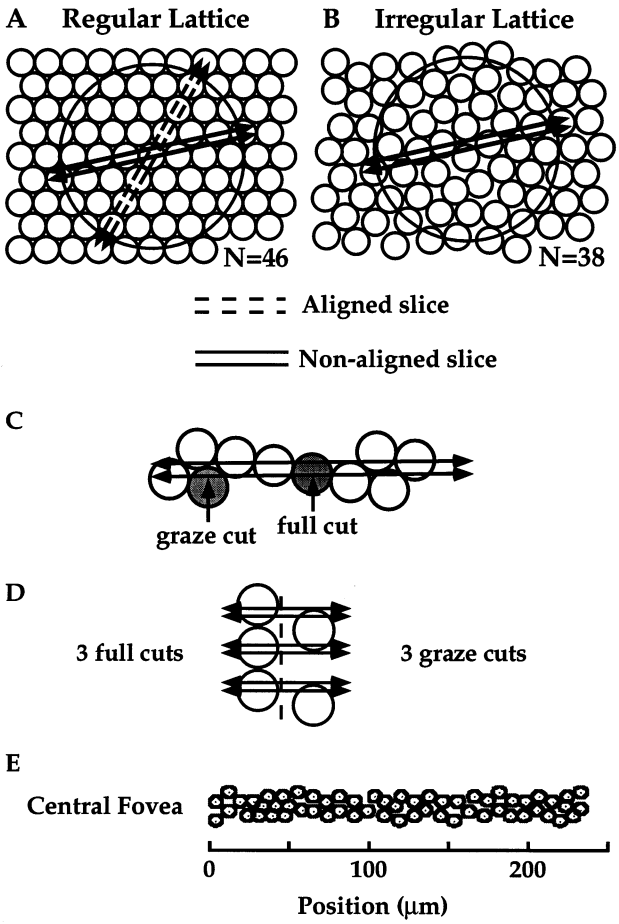

Fig. A1. Problems in measuring cone packing density from vertical tissue sections. (A) Effect of tissue slice orientation on cone density estimates. The dashed lines represent a slice that is aligned with a row of cones and the solid lines a slice that is not aligned with a row of cones. The aligned slice intersects seven cones and the non-aligned slice ten cones across the same distance; (B) effect of cone lattice irregularity on cone density estimates. The non-aligned tissue slice and circle from A are shown again. The number of cones intersected in the slices are identical, however, the regular lattice contains 46 cones whereas the irregular lattice contains only 38; (C) schematic illustrating graze and full cuts through photoreceptors. The parallel arrows represent the 2 mm tissue section. The shaded cones have been sliced near the edge (graze cut) and near the center (full cut); (D) schematic illustrating two scenarios for tissue sectioning. On the left, three cones have been sliced near their centers thereby producing three full cuts. On the right, two cones have been sliced near their edges producing three graze cuts. The same number of cones would be visible in the three tissue sections even though there were actually three cones in one scenario and two in the other. The scenario on the left would be assigned a higher likelihood than the one on the right because it is consistent with a more tightly-packed, regular hexagonal cone lattice; (E) the foveal cone lattice arrangement that produced the maximum likelihood. The cones are plotted in their 2-dimensional positions within the area contained in the three tissue sections.

of the sections using the following procedure. First, individual cones were catalogued and their position along the long axis of the section was determined; these positions were placed into a database. Second, each catalogued cone in each section was categorized as a full or graze cut. It was not possible to deduce from the photographs whether the graze-cut receptors were at the front or back of a section, so we could not determine whether the center of a cone was in front of or behind a section. Third, the relative positions of the three sections were varied in the database; each possible combination of full and graze cuts across the three sections was assigned a likelihood (Fig. A1, part D) and the relative positions of the sections that yielded the maximum likelihood was found. The likelihood had a clear maximum, so the correct relative positions of the sections were easily determined.

The foveal lattice shown in part E of Fig. A1 was reconstructed from the positioning of the sections yielding the highest likelihood. This solution corresponds to a cone packing density of 15000 cones/mm^2 in the center of the fovea. This value is significantly lower than the value of 18921 cones/mm^2 reported by Yuodelis and Hendrickson [2] and supports our conjecture that they over-estimated packing density. The cone density estimate at eccentricities of 5 and 10° were 21500 and 12500 cones/mm^2, respectively.

References

[1] Abramov I, Gordon J, Hendrickson A, Hainline L, Dobson V, Laboissiere E. The retina of the newborn human infant. Science 1982;217:265–7.

[2] Yuodelis C, Hendrickson AE. A qualitative and quantitative analysis of the human fovea during development. Vis Res 1986;26:847–55.

[3] Banks MS, Salapatek P. Acuity and contrast sensitivity in 1-, 2-, and 3-month-old human infants. Invest Ophthalmol Vis Sci 1978;17:361–5.

[4] Dobson V, Teller DY. Visual acuity in human infants: a review and comparison of behavioral and electrophysiological studies. Vis Res 1978;18:1469–83.

[5] Hendrickson AE, Drucker D. The development of parafoveal and mid-peripheral human retina. Behav Brain Res 1992;49:21–31.

[6] Hendrickson AE, Yuodelis C. The morphological development of the human fovea. Ophthalmology 1984;91:603–12.

[7] Banks MS. Infant form vision: the MTF. Ph.D. thesis, University of Minnesota, 1976.

[8] Bronson G. The postnatal growth of visual capacity. Child Dev 1974;45:873–90.

[9] Brown AM. Intrinsic noise and infant visual performance. In: Simons K, editor. Early Visual Development: Normal and Abnormal. New York: Oxford University, 1993.

[10] Brown AM, Dobson V, Maier J. Visual acuity of human infants at scotopic, mesopic and photopic luminances. Vis Res 1987;27:1845–58.

[11] Candy TR, Banks MS, Hendrickson AE, Crowell JA. Neonatal vision and cone properties in fovea and periphery. Invest Ophthalmol Vis Sci (Suppl) 1993;34:1356.

[12] Sokol S, Moskowitz A, McCormack G, Augliere R. Infant grating acuity is temporally tuned. Vis Res 1988;28:1357–66.

[13] Packer O, Hartmann EE, Teller DY. Infant color vision: The effect of test field size on Rayleigh discrimination. Vis Res 1984;24:1247–60.

[14] Salapatek P. Pattern perception in early infancy. In: Cohen LB, Salapatek P, editors. Infant Perception: From Sensation to Cognition. New York: Academic Press, 1975.

[15] Banks MS, Bennett PJ. Optical and photoreceptor immaturities limit the spatial and chromatic vision of human neonates. J Optical Soc Am A 1988;5:2059–79.

[16] Miller WH, Bernard GD. Averaging over the foveal receptor aperture curtails aliasing. Vis Res 1983;23:1365–9.

[17] Curcio CA. Diameters of presumed cone apertures in human retina. In Annual Meeting of the Optical Society of America 1987:1–11.

[18] Wilson HR. Development of spatiotemporal mechanisms in infant vision. Vis Res 1988;28:611–28.

[19] Banks MS, Geisler WS, Bennett PJ. The physical limits of grating visibility. Vis Res 1987;27:1915–24.

[20] Howell ER. The functional area for summation to threshold for sinusoidal gratings. Vis Res 1978;18:369–74.

[21] Sekiguchi N, Williams DR, Brainard DH. Aberration-free measurements of the visibility of isoluminant gratings. J Optical Soc Am A 1993;10:2105–17.

[22] Banks MS, Crowell JA. A re-examination of two analyses of front-end limitations to infant vision. In: Simons K, editor. Early Visual Development: Normal and Abnormal. New York: Oxford University Press, 1993.

[23] Brown AM. Development of visual sensitivity to light and color vision in human infants: A critical review. Vis Res 1990;30:1159–88.

[24] Wilson HR. Theories of infant visual development. In: Simons K, editor. Early Visual Development: Normal and Abnormal. New York: Oxford University, 1993.

[25] Banks MS, Sekuler AB, Anderson SJ. Peripheral spatial vision: Limits imposed by optics, photoreceptors, and receptor pooling. J Optical Soc Am A 1991;8:1775–87.

[26] Wässle H, Grünert U, Röhrenbeck J, Boycott BB. Retinal ganglion cell density and cortical magnification factor in the primate. Vis Res 1990;30:1897–911.

[27] Green DM, Swets JA. Signal Detection Theory and Psychophysics. New York: Wiley, 1966.

[28] Bone RA, Landrum JT, Fernandez L, Tarsis SL. Analysis of the macular pigment by HPLC: retinal distribution and age study. Invest Ophthalmol Vis Sci 1988;29:843–9.

[29] Werner JS. Development of scotopic sensitivity and the absorption spectrum of the human ocular media. J Optical Soc Am 1982;72:247–58.

[30] Hansen RM, Fulton AB. Psychophysical estimates of ocular media density of human infants. Vis Res 1989;29:687–90.

[31] Boettner E and Wolter M. Transmission of the ocular media. Air Force Technical Documentary Report No.MRL-TDR-62-34, 1962.

[32] Wyszecki G, Stiles WS. Color Science: Concepts and Methods, Quantitative Data and Formulae. New York: Wiley, 1982.

[33] Shannon E, Skoczenski AM, Banks MS. Retinal illuminance and contrast sensitivity in human infants. Vis Res 1996;36:67–76.

[34] Navarro R, Artal P, Williams DR. Modulation transfer of the human eye as a function of retinal eccentricity. J Optical Soc Am A 1993;10:201–12.

[35] Cook RC, Glasscock RE. Refractive and ocular findings in the newborn. Am J Ophthalmol 1951;34:1407–13.

[36] Bonds AB, Freeman RD. Development of optical quality in the kitten eye. Vis Res 1978;18:391–8.

[37] Campbell FW, Gubisch RW. Optical quality of the human eye. J Physiol 1966;186:558–78.

[38] Larsen JS. The sagittal growth of the eye. IV. Ultrasonic measurement of the axial length of the eye from birth to puberty. Acta Ophthalmol 1971;49:873–86.

[39] MacLeod DIA, Williams DR, Makous W. A visual nonlinearity fed by single cones. Vis Res 1992;32:347–63.
[40] Williams DR. Visibility of interference fringes near the resolution limit. J Optical Soc Am A 1985;2:1087–93.
[41] Curcio CA, Sloan KR, Kalina RE, Hendrickson AE. Human photoreceptor topography. J Comp Neurol 1990;292:497–523.
[42] Anderson SJ, Hess RF. Post-receptoral undersampling in normal human peripheral vision. Vis Res 1990;30:1507–15.
[43] Galvin SJ, Williams DR, Coletta NJ. The spatial grain of motion perception in human peripheral vision. Vis Res 1996;36:2283–95.
[44] Thibos LN, Cheney FE, Walsh DJ. Retinal limits to the detection and resolution of gratings. J Optical Soc Am A 1987;4:1524–9.
[45] Aslin RN. Anatomical constraints on oculomotor development: implications for infant perception. In: Yonas A, editor. Perceptual Development in Infancy: The Minnesota Symposia on Child Psychology, vol. 20. Hillsdale: Lawrence Erlbaum Associates, 1988.
[46] Hamasaki DI, Sutija VG. Development of X- and Y-cells in kittens. Exp Brain Res 1979;35:9–23.
[47] Rusoff AC, Dubin MW. Kitten ganglion cells: dendritic field size at 3 weeks of age and correlation with receptive field size. Invest Ophthalmol Vis Sci 1978;17:819–21.
[48] Blakemore C, Vital-Durand F. Organization and post-natal development of the monkey's lateral genicular nucleus. J Physiol 1986;380:453–90.
[49] Banks MS, Salapatek P. Infant visual perception. In: Mussen P, editor. Handbook of Child Psychology. New York: Wiley, 1983.
[50] Norcia AM, Tyler CW, Hamer RD. Development of contrast sensitivity in the human infant. Vis Res 1990;30:1475–86.
[51] Van Nes F, Bouman M. Spatial modulation transfer in the human eye. J Optical Soc Am 1967;57:401–6.
[52] Daitch JM, Green DG. Contrast sensitivity of the human peripheral retina. Vis Res 1969;9:947–52.
[53] Koenderink JJ, Bouman MA, Bueno de Mesquita AE, Slappendel S. Perimetry of contrast detection thresholds of moving spatial sine wave patterns. IV. The influence of the mean retinal illuminance. J Optical Soc Am A 1978;68:860–5.
[54] Allen D, Tyler CW, Norcia AM. Development of grating acuity and contrast sensitivity in the central and peripheral visual field of the human infant. Vis Res 1996;36:1945–53.
[55] Lewis TL, Maurer D, Kaye D. Newborns' central vision: Whole or hole? J Exp Child Psychol 1978;26:193–203.
[56] Lewis TL, Maurer D. The development of the temporal and nasal visual fields during infancy. Vis Res 1992;32:903–11.
[57] Sireteanu R, Fronius M, Constantinescu DH. The development of visual acuity in the peripheral visual field of human infants-binocular and monocular measurements. Vis Res 1994;34:1659–71.
[58] Sireteanu R, Kellerer R, Boergen KP. The development of peripheral visual acuity in human infants. A preliminary study. Hum Neurobiol 1984;3:81–5.
[59] Spinelli D, Pirchio M, Sandini G. Visual acuity in the young infant is highest in a small retinal area. Vis Res 1983;23:1133–6.
[60] Diaz-Araya C, Provis JM. Evidence of photoreceptor migration during early foveal development: A quantitative analysis of human fetal retinae. Vis Neurosci 1992;8:505–14.
[61] Stenstrom S. Investigation of the variation and the correlation of the optical elements of human eyes. Am J Optom 1946;25:5.